

Thick branes with inner structure in mimetic $f(R)$ gravity

Jing Chen^{a b}, Wen-Di Guo^{a b c}, and Yu-Xiao Liu^{a b d *}

^aJoint Research Center for Physics,
Lanzhou University and Qinghai Normal University,
Lanzhou 730000 and Xining 810000, P. R. China

^bInstitute of Theoretical Physics & Research Center of Gravitation,
Lanzhou University, Lanzhou 730000, P. R. China

^cCentro de Astrofísica e Gravitação - CENTRA,
Departamento de Física,
Instituto Superior Técnico - IST,
Universidade de Lisboa - UL,

Av. Rovisco Pais 1, 1049-001 Lisboa, Portugal

^dKey Laboratory for Magnetism and Magnetic of the Ministry of Education,
Lanzhou University, Lanzhou 730000, P. R. China

In this paper, we study the structure and gravitational resonances of thick branes generated by a mimetic scalar field in $f(R)$ gravity. We obtain several typical thick brane solutions for $f(R) = R + \alpha R^2$. To study their stability, we analyze the tensor perturbation of the metric. It is shown that any thick brane model with $df/dR > 0$ is stable and the graviton zero mode can be localized on the brane for each solution, which indicates that the four-dimensional Newtonian gravity can be restored. The effect of the parameter α on the gravitational resonances is studied. As a brane splits into multi sub-branes, the effective potential of the tensor perturbation will have an abundant inner structure with multi-wells, and this will lead to new phenomena of the gravitational resonances.

PACS numbers:

I. INTRODUCTION

In last twenty years, brane world scenario has been an attractive topic and researched widely. Arkani-Hamed, Dimopoulos, and Dvali (ADD) provided an alternative solution to gauge hierarchy problem with a large extra dimension brane model [1]. In ADD model, all matter fields are confined on a four-dimensional brane which is embedded in a higher-dimensional spacetime, only the gravity can propagate in the bulk. After that, Randall and Sundrum proposed two different kinds of extra dimension models, RS-1 [2] and RS-2 model [3]. In RS-1 model the extra dimension is compact and warped but in RS-2 model the scale of the warped extra dimension is infinite. In RS-2 model, the four-dimensional Newtonian potential can be restored even if the extra dimension is infinite. However, the thicknesses of the brane of RS models are neglected, and this is the reason why we called them thin brane models. Combining the RS-2 model with the domain wall model [4] one can generalize the RS-2 model to a thick brane model [5–7]. The localization problem of matter fields on a thick brane was studied in Refs. [5, 7–15]. And cosmology issues in brane world models were also investigated in [16–21]. In thick brane world scenario, the brane is usually generated by a canonical scalar field [22–27]. Furthermore, various kinds of thick branes generated by multi-scalar fields also were

investigated widely [28–31].

On the other hand, it is well known that general relativity still has some problems. For example, in terms of astronomical observations, it cannot explain the early-time inflation [32], the late-time acceleration [33], and the issue of the rotation curve of a disc galaxy [34], etc; and in terms of theory, it is not renormalizable. To solve the issues indicated by astronomical observations, physicists provided two kinds of schemes, one is assuming the existence of extra energy and matter, the other one is modifying general relativity to match observations. Mimetic gravity is a modified theory proposed by Chamseddine and Mukhanov [35]. In this theory the conformal degree of freedom of the background metric is isolated and it could mimic cold dark matter [36–42]. On the other hand, instead of the extra scalar field this conformal degree of freedom can also mimic the scalar field which generates the thick brane. In last few years, Y. Zhong et al. investigated thick branes generated by the mimetic scalar field in Ref. [43]. And it was found that one could construct some exact solutions of brane world, and some of them have inner structure. This inner structure in a thick brane can lead to new phenomena in the gravitational resonances, which were further investigated in Ref. [44].

Because $f(R)$ gravity is a simple renormalizable higher-order gravity theory [45, 46] which could explain the inflation [47–52] and the late-time acceleration [53–61], Nojiri and Odintsov generalized mimetic gravity to mimetic $f(R)$ gravity in 2014 [62]. Leon and Saridakis studied the dynamical behavior of mimetic $f(R)$ grav-

*liuyx@lzu.edu.cn, corresponding author

ity [63]. Odintsov and Oikonomou investigated dark energy oscillations in this gravity [64]. As a higher-order gravity, the ghost stability should be considered, and the authors of Ref. [41] found that, for positive energy density of the mimetic fluid in cosmology, mimetic $f(R)$ gravity is free of ghost instability. Myrzakulov studied the stability of de Sitter solution in this theory [65]. As studied in Refs. [43, 44], the mimetic scalar field can generate thick branes, so we would like to study the properties of thick branes in mimetic $f(R)$ gravity. Taking $f(R) = R + \alpha R^2$ as an example, we want to know effect of the second term. The stability of the tensor perturbation of this system is an important issue, with which the important phenomena of gravitational resonances can be investigated. These gravitational resonances will have experimental signals in high energy collider and will also contribute to the correction of the four-dimensional gravity potential. We also note that, thin brane scenario in mimetic $f(R)$ gravity was investigated in Ref. [66], thick brane in mimetic $f(T)$ gravity was studied in Ref. [67], and thick branes with inner structure in the generalized hybrid metric-Palatini gravity were studied in Ref. [68].

The organization of our work is as follows. In Sec. II, we review mimetic $f(R)$ theory and construct three flat thick brane models with $f(R) = R + \alpha R^2$. In Sec. III, we investigate the tensor perturbation and the graviton zero mode in each brane model. In Sec. IV we study the gravitational resonances, and show the abundant behavior of these resonances due to inner structure of the branes. Finally, in Sec. V we come to the conclusions and discussions.

II. MIMETIC $f(R)$ GRAVITY AND THICK BRANE MODELS

First, we will give a brief review of thick brane in mimetic $f(R)$ theory. The original mimetic scalar comes from the conformal degree freedom of the metric [35]. Later, it was generalized to a Lagrange multiplier method equivalently [36]. In this paper, we will use the Lagrange multiplier method. The action of mimetic $f(R)$ gravity in a five-dimensional spacetime is

$$S = \int d^4x dy \sqrt{-g} \left[\frac{1}{2} f(R) + L_\phi \right], \quad (1)$$

where $f(R)$ is a function of the scalar curvature R . Note that, we have taken $\kappa^2 = 1$. The Lagrangian of the mimetic scalar field is

$$L_\phi = \lambda [g^{MN} \partial_M \phi \partial_N \phi - U(\phi)] - V(\phi), \quad (2)$$

where λ is the Lagrange multiplier. The field equations can be obtained by varying action (1) with respect to the metric g_{MN} , the scalar field ϕ , and the Lagrange

multiplier λ , respectively:

$$f_R R_{MN} - \frac{1}{2} g_{MN} f + (g_{MN} \square^{(5)} - \nabla_M \nabla_N) f_R = g_{MN} L_\phi - 2\lambda \partial_M \phi \partial_N \phi, \quad (3)$$

$$2\lambda \square^{(5)} \phi + 2\nabla_M \lambda \nabla^M \phi + \lambda \frac{\partial U}{\partial \phi} + \frac{\partial V}{\partial \phi} = 0, \quad (4)$$

$$g^{MN} \partial_M \phi \partial_N \phi - U(\phi) = 0, \quad (5)$$

where $\square^{(5)} = g^{MN} \nabla_M \nabla_N$ is the five-dimensional d'Alembert operator and $f_R \equiv df(R)/dR$. The indices $M, N, \dots = 0, 1, 2, 3, 5$ and $\mu, \nu, \dots = 0, 1, 2, 3$ denote the bulk and brane coordinates, respectively. In the original mimetic gravity, $U(\phi) = -1$ [35]. Later, it was generated as $U(\phi) \neq -1$ by Astashenok, Odintsov and Oikonomou [69]. In order to generate a thick brane, the mimetic scalar field should be spacelike and only depends on the extra dimension y [43]. So from Eq. (5) we know that, $U(\phi) = g^{MN} \partial_M \phi \partial_N \phi > 0$.

In this paper we consider the four-dimensional flat brane with the metric

$$ds^2 = a^2(y) \eta_{\mu\nu} dx^\mu dx^\nu + dy^2, \quad (6)$$

where $a(y)$ is the warp factor, y represents the extra dimension, and $\eta_{\mu\nu}$ is the four-dimensional Minkowski metric. With this metric, Eqs. (3)-(5) can be written as

$$f + \frac{6a'^2}{a^2} f_R + \frac{2a''}{a} f_R - \frac{6a'}{a} f'_R - 2f''_R - 2V - 2\lambda (U - \phi'^2) = 0, \quad (7)$$

$$f + \frac{8a''}{a} f_R - \frac{8a'}{a} f'_R - 2V - 2\lambda (U + \phi'^2) = 0, \quad (8)$$

$$\frac{\partial V}{\partial \phi} + 2\lambda' \phi' + \lambda \left(\frac{\partial U}{\partial \phi} + 8\phi' \frac{a'}{a} + 2\phi'' \right) = 0, \quad (9)$$

$$U(\phi) - \phi'^2 = 0, \quad (10)$$

and

$$R = -12 \frac{a'^2}{a^2} - 8 \frac{a''}{a}, \quad (11)$$

where the symbol prime denotes the derivative with respect to the extra dimension coordinate y . Combining Eqs. (7), (8), and (10), we can get

$$\lambda = \frac{1}{\phi'^2} \left(\frac{3a''}{2a} f_R - \frac{3a'^2}{2a^2} f_R - \frac{a'}{2a} f'_R + \frac{1}{2} f''_R \right), \quad (12)$$

$$V = \frac{f}{2} + \frac{3a'^2}{a^2} f_R + \frac{a''}{a} f_R - \frac{3a'}{a} f'_R - f''_R. \quad (13)$$

Note that, there are only three independent equations in Eqs. (7)-(10), because the left side of Eq. (3) is divergent-free [46]. Since there are six functions: $f(R)$, $a(y)$, $\phi(y)$, $\lambda(\phi)$, $V(\phi)$, and $U(\phi)$, we should fix three of them. In this paper, we will give $f(R)$, $a(y)$, and $\phi(y)$, and solve $\lambda(\phi)$, $V(\phi)$, and $U(\phi)$.

We will consider $f(R) = R + \alpha R^2$ as an example, where α is the parameter which measures the degree of deviation from mimetic gravity. In this formula of $f(R)$ we require

$$f_R > 0 \quad (14)$$

in the whole extra dimension in order to guarantee that the graviton is not a ghost [46]. Then we will give three kinds of warp factors to study behavior of gravitational resonances.

A. Model 1

In the first model, the warp factor and the scalar field are set as follows

$$a(y) = \operatorname{sech}^n(ky), \quad (15)$$

$$\phi(y) = v \tanh^n(ky), \quad (16)$$

where n is a positive odd integer, v is a positive parameter. Shapes of the warp factor and the scalar field for different n are depicted in Figs. 1(a) and 1(b), respectively. From Fig. 1(b), we can see that the scalar field is a single-kink and a double-kink for $n = 1$ and $n \geq 3$, respectively. Besides, it can be noticed that as n increases the platform near $y = 0$ of the double-kink scalar field becomes wider and the warp factor becomes more concentrated.

We can solve U , V , and λ from Eqs. (10)-(13) as a function of ϕ ,

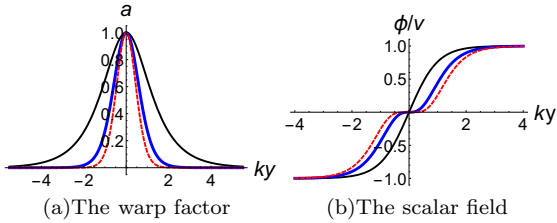


FIG. 1: Shapes of the warp factor $a(y)$ and the scalar field $\phi(y)$ in model 1. The parameters are set as $n = 1$ for the black lines, $n = 3$ for the thick blue lines, and $n = 5$ for the dashed red lines.

$$U(\phi) = k^2 n^2 v^2 \tilde{\phi}^{\frac{2(n-1)}{n}} \left(\tilde{\phi}^{\frac{2}{n}} - 1 \right)^2, \quad (17)$$

$$V(\phi) = k^2 n \left(8\alpha k^2 (n+1)(n+6)(5n+2) \tilde{\phi}^4 \right. \\ \left. - (8\alpha k^2 (n(37n+56)+16)+6n+3) \tilde{\phi}^2 \right. \\ \left. + 32k^2(\alpha+3\alpha n)+3 \right), \quad (18)$$

$$\lambda(\phi) = \frac{\tilde{\phi}^{2-2n}}{2nv^2(1-\tilde{\phi}^2)^2} \left(8\alpha k^2 (5n+2)(n(3n+2)-6) \tilde{\phi}^4 \right. \\ \left. + (3-32\alpha k^2(n(4n-9)-4)) \tilde{\phi}^2 \right. \\ \left. - (16\alpha k^2(5n+2)+3) \right), \quad (19)$$

$$\text{where } \tilde{\phi} = \frac{\phi}{v}.$$

Considering the condition (14) in this model, we obtain the range of $k^2\alpha$:

$$-\frac{1}{16n} < k^2\alpha < \frac{1}{40n^2}. \quad (20)$$

Here we show the shapes of the dimensionless energy density ρ/k^2 in Fig. 2 for several situations. Besides, it is found that the brane will split into two sub-branes when $-\frac{1}{16n} < k^2\alpha < -\frac{1}{8n(4+5n)}$.

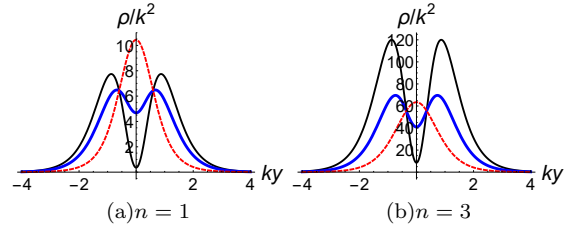


FIG. 2: The energy density of model 1 with $v = 1$, and $n = 1$ (the left panel) and $n = 3$ (the right panel). In the left panel we set $k^2\alpha = -0.06$ for the black line, $k^2\alpha = -0.03$ for the thick blue line, and $k^2\alpha = 0.01$ for the dashed red line. In the right panel we set $k^2\alpha = -0.018$ for the black line, $k^2\alpha = -0.0073$ for the thick blue line, and $k^2\alpha = 0.00014$ for the dashed red line.

B. Model 2

In the second model, the warp factor has a platform near the origin of the extra dimension, which can be seen from Fig. 3. The scalar field is a single-kink configuration. The expressions of the warp factor, the scalar field, and the scalar field potential U are given by

$$a(y) = \tanh[k(y+b)] - \tanh[k(y-b)], \quad (21)$$

$$\phi(y) = v \tanh(ky), \quad (22)$$

$$U(\phi) = \frac{k^2}{v^2} (\phi^2 - v^2)^2. \quad (23)$$

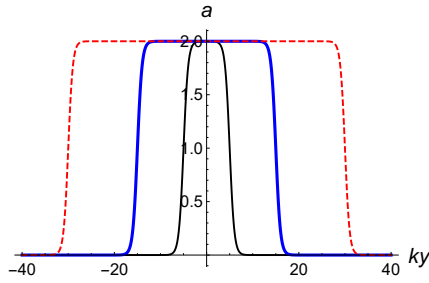


FIG. 3: The warp factor of model 2. The parameter v is set to $v = 1$, and $kb = 5$ for the black line, $kb = 15$ for the thick blue line, and $kb = 30$ for the dashed red line.

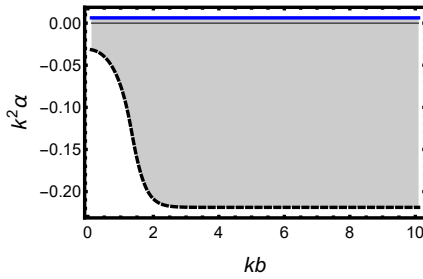


FIG. 4: Plot of the range (the dark region) of $k^2\alpha$ and kb in the condition of $f_R > 0$ for model 2.

Here we do not show the complicated $V(\phi)$ and $\lambda(\phi)$, which can be solved analytically. Note that the width of the platform of the warp factor is controlled by the parameter kb . Considering the condition (14), we can obtain numerically the range of the parameter $k^2\alpha$, which is shown in Fig. 4. From this figure, we can see that when $kb \gtrsim 2$ the range of $k^2\alpha$ is of about

$$-0.219 < k^2\alpha < 0.00625. \quad (24)$$

The dimensionless energy density ρ/k^2 in this model is shown in Fig. 5. The brane will split into multi-branes for $kb \gtrsim 2$ and all allowed $k^2\alpha$ in the range we obtained.

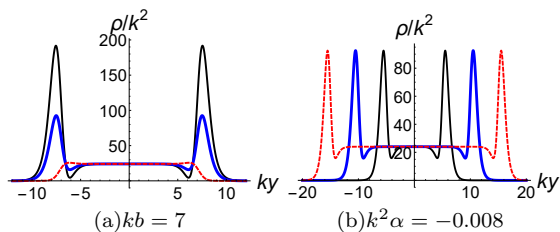


FIG. 5: The energy density of model 2. The parameter v is set to $v = 1$. In the left panel, we set $kb = 7$, and $k^2\alpha = -0.018$ for the black line, $k^2\alpha = -0.008$ for the thick blue line, and $k^2\alpha = 0.006$ for the dashed red line. In the right panel, we set $k^2\alpha = -0.008$, and $kb = 5$ for the black line, $kb = 10$ for the thick blue line, and $kb = 15$ for the dashed red line.

When kb close to zero the warp factor and the energy density will close to model 1 with $n = 1$. In other words, whether the brane split or not depends on the value of $k^2\alpha$, when $k^2\alpha$ is smaller than some value the brane will split into two sub-branes.

We can also extend this warp factor to the form as follows

$$a(y) = \tanh[k(y - b - d)] - \tanh[k(y + b + d)] - \tanh[k(y + d)] + \tanh[k(y - d)], \quad (25)$$

where b and d are positive parameters. Using this warp factor one can construct a brane world with double number of sub-branes, which will be further investigated in Sec. IV.

C. Model 3

The third model is

$$a(y) = \operatorname{sech}(k(y - b)) + \operatorname{sech}(ky) + \operatorname{sech}(k(y + b)), \quad (26)$$

$$\phi(y) = vtanh(ky), \quad (27)$$

$$U(\phi) = \frac{k^2}{v^2}(\phi^2 - v^2)^2. \quad (28)$$

The scalar field is also a single-kink and the warp factor has peaks for large parameter kb , which can be seen from Fig. 6(a). Here we also do not show the complicated expressions of $\lambda(\phi)$ and $V(\phi)$.

The range of $k^2\alpha$ due to the condition $f_R > 0$ is shown in Fig. 7. We can see that for $kb \gtrsim 4$, the range of $k^2\alpha$ is $-0.0625 < k^2\alpha < 0.025$. The dimensionless energy density ρ/k^2 for $kb = 5$ in this model is shown in Fig. 6(b). In this situation, the sub-branes will always exist for $kb \gtrsim 4$ and all $k^2\alpha$ in the range we obtained. When kb close to zero, the warp factor and the energy density will also close to model 1 with $n = 1$. In other words, whether the brane split or not for the case of small kb depends on the value of $k^2\alpha$. When $k^2\alpha$ less than some critical value the brane will split into two sub-branes.

We can also extend this three-peak model to multiple-peak model with the following warp factor

$$a(y) = \sum_{n=-N}^N \operatorname{sech}(k(y + nb)), \quad (29)$$

where N is an arbitrary positive integer.

III. TENSOR PERTURBATIONS AND LOCALIZATION

In this section, we investigate the stability of the system through studying the tensor perturbation. The perturbed metric is given by

$$g_{MN} = \bar{g}_{MN} + \delta g_{MN}, \quad (30)$$

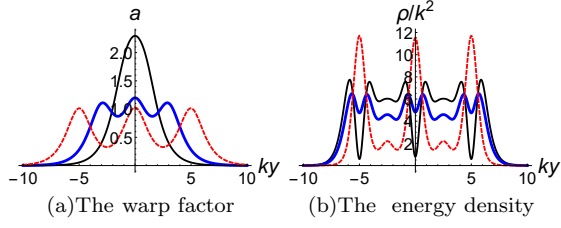


FIG. 6: The warp factor and the energy density of model 3. The parameter v is set to $v = 1$. In the left panel we set $kb = 1$ for the black line, $kb = 3$ for the thick blue line, and $kb = 5$ for the dashed red line. In the right panel we set $kb = 5$ and $k^2\alpha = -0.06$ for the black line, $k^2\alpha = -0.03$ for the thick blue line, and $k^2\alpha = 0.02$ for the dashed red line.

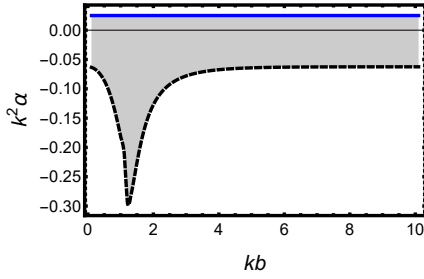


FIG. 7: Plot of the range (the dark region) of $k^2\alpha$ and kb in the condition of $f_R > 0$ for model 3.

with

$$\bar{g}_{MN} = \begin{pmatrix} a^2(y)\eta_{\mu\nu} & 0 \\ 0 & 1 \end{pmatrix}, \quad \delta g_{MN} = \begin{pmatrix} a^2(y)h_{\mu\nu} & 0 \\ 0 & 0 \end{pmatrix}, \quad (31)$$

where $h_{\mu\nu} = h_{\mu\nu}(x^\rho, y)$ depends on all coordinates. Here, we only consider the tensor perturbation, so $\delta g_{5N} = 0$. Using the relation $g^{NP}g_{PM} = \delta_M^N$, one can obtain the inverse of δg_{MN} ,

$$\delta g^{MN} = \begin{pmatrix} -a^{-2}(y)h^{\mu\nu} & 0 \\ 0 & 0 \end{pmatrix}, \quad (32)$$

where $h^{\mu\nu} = \eta^{\mu\lambda}\eta^{\nu\rho}h_{\lambda\rho}$. Note that, we only keep the first order. Then the following relations can be obtained

$$\begin{aligned} \delta R_{\mu\nu} = & -\frac{1}{2} \left(\square^{(4)}h_{\mu\nu} + \partial_\mu\partial_\nu h - \partial_\nu\partial_\sigma h_\mu^\sigma - \partial_\mu\partial_\sigma h_\nu^\sigma \right) \\ & - 2aa'h'_{\mu\nu} - 3h_{\mu\nu}a'^2 - ah_{\mu\nu}a'' - \frac{1}{2}a^2h''_{\mu\nu} \\ & - \frac{1}{2}a\eta_{\mu\nu}a'h', \end{aligned} \quad (33)$$

$$\delta R_{\mu 5} = \frac{1}{2}\partial_y(\partial_\lambda h_\mu^\lambda - \partial_\mu h), \quad (34)$$

$$\delta R_{55} = -\frac{1}{2} \left(\frac{2a'h'}{a} + h'' \right), \quad (35)$$

$$\delta R = -\frac{\square^{(4)}h}{a^2} + \frac{\partial_\mu\partial_\nu h^{\mu\nu}}{a^2} - \frac{a'}{a}5h' - h''. \quad (36)$$

Here $\square^{(4)} = \eta^{\mu\nu}\partial_\mu\partial_\nu$ is the four-dimensional d'Alembert operator, and $h = \eta^{\mu\nu}h_{\mu\nu}$ is the trace of the tensor perturbation. Hereafter, we will use the transverse-traceless gauge $h = 0 = \partial_\mu h_\nu^\mu$. Then, Eqs. (33)-(36) can be simplified further. Using the above relations, we obtain the tensor perturbation equation

$$\begin{aligned} & -\frac{1}{4}a^2h_{\mu\nu}f(R) + \frac{1}{2}a^2h_{\mu\nu}V - \frac{1}{2}\lambda a^2h_{\mu\nu}[\phi'^2 - U(\phi)] \\ & + \frac{1}{2} \left(-\frac{1}{2}\square^{(4)}h_{\mu\nu} - 3a'^2h_{\mu\nu} - 2aa'h'_{\mu\nu} - aa''h_{\mu\nu} \right. \\ & \left. - \frac{a^2}{2}h''_{\mu\nu} \right) f_R + a^2 \left[\frac{1}{2}h_{\mu\nu} \left(3\frac{a'}{a}f'_R + f''_R \right) - \frac{1}{4}h'_{\mu\nu}f'_R \right] = 0. \end{aligned} \quad (37)$$

Comparing with the Einstein equation (3), one can easily obtain

$$\left(a^{-2}\square^{(4)}h_{\mu\nu} + 4\frac{a'}{a}h'_{\mu\nu} + h''_{\mu\nu} \right) f_R + h'_{\mu\nu}f'_R = 0. \quad (38)$$

After the coordinate transformation $dz = a^{-1}dy$, we can rewrite the perturbed equation (38) as

$$\left[\partial_z^2 + \left(3\frac{\partial_z a}{a} + \frac{\partial_z f_R}{f_R} \right) \partial_z + \square^{(4)} \right] h_{\mu\nu} = 0. \quad (39)$$

Considering the decomposition $h_{\mu\nu}(x^\rho, z) = (a^{-3/2}f_R^{-1/2})\epsilon_{\mu\nu}(x^\rho)\psi(z)$, where $\epsilon_{\mu\nu}(x^\rho)$ satisfies the transverse and traceless conditions $\eta^{\mu\nu}\epsilon_{\mu\nu} = 0$ and $\partial_\mu\epsilon_\nu^\mu = 0$, we obtain the following Schrödinger-like equation for the extra-dimensional part $\psi(z)$

$$[-\partial_z^2 + W(z)]\psi(z) = m^2\psi(z), \quad (40)$$

where

$$\begin{aligned} W(z) = & \frac{3}{4}\frac{(\partial_z a)^2}{a^2} + \frac{3}{2}\frac{\partial_z a}{a}\frac{\partial_z f_R}{f_R} \\ & - \frac{1}{4}\frac{(\partial_z f_R)^2}{f_R^2} + \frac{3}{2}\frac{\partial_z^2 a}{a} + \frac{1}{2}\frac{\partial_z^2 f_R}{f_R}, \end{aligned} \quad (41)$$

is the effective potential of gravitons. The effective potential (41) in y coordinate is

$$W(z(y)) = \frac{9}{4}a'^2 + 2\frac{aa'f'_R}{f_R} - \frac{1}{4}a^2\frac{f''_R}{f_R^2} + \frac{3}{2}ad'' + \frac{1}{2}\frac{a^2f''}{f_R}. \quad (42)$$

It would be clearer if Eq. (40) is written in the following form

$$QQ^\dagger\psi(z) = m^2\psi(z), \quad (43)$$

with

$$Q = \partial_z + \left(\frac{3}{2}\frac{\partial_z a}{a} + \frac{1}{2}\frac{\partial_z f_R}{f_R} \right), \quad (44)$$

$$Q^\dagger = -\partial_z + \left(\frac{3}{2}\frac{\partial_z a}{a} + \frac{1}{2}\frac{\partial_z f_R}{f_R} \right). \quad (45)$$

Equation (43) guarantees that there is no tachyonic graviton with $m^2 < 0$. So, the system is stable under the tenser perturbation.

The solution of the graviton zero mode is

$$\psi^{(0)}(z) = N_0 a^{3/2}(z) f_R^{1/2}(z), \quad (46)$$

where N_0 is the normalization constant. It is easy to show that $\psi^{(0)}(z)$ is normalizable, i.e.,

$$\int_{-\infty}^{\infty} |\psi^{(0)}(z)|^2 dz < \infty. \quad (47)$$

This means that the graviton zero mode for each model considered in this paper can be localized near the brane¹ [6, 70]. The effective potentials and the graviton zero modes for the three models are shown in Fig. 8. From the analysis above of this section we notice that the tenser perturbation in mimetic $f(R)$ gravity is the same as that in $f(R)$ gravity [71]. The reason is that the tenser perturbation is independent of the mimetic scalar field. And this result is also consistent with mimetic brane world [43]. But the mimetic scalar field gives a degree of freedom which could generate more abundant inner structure.

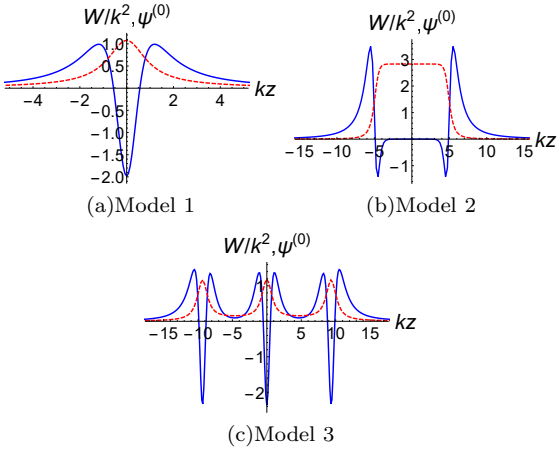


FIG. 8: The effective potentials (the blue lines) and the corresponding graviton zero modes (the red dashed lines) for the three models. For model 1, we set $v = 1$ and $k^2\alpha = 0.01$; for model 2, $v = 1$, $kb = 10$, and $k^2\alpha = 0.006$; and for model 3, $v = 1$, $kb = 5$, and $k^2\alpha = 0.02$.

¹ Actually, $QQ^\dagger\psi(z) = 0$ has another solution:

$$\psi^{(0)}(z) = M_0 a^{3/2}(z) f_R^{1/2}(z) \int \frac{1}{a^3(z) f_R(z)} dz.$$

But this solution is divergent at $z \rightarrow \pm\infty$ for each model we considered, so it was abandoned.

IV. THE GRAVITATIONAL RESONANCES OF MIMETIC $f(R)$ BRANE

The abundant inner structure of the effective potential may lead to some interesting resonant behavior which will be studied in this section.

To get numerical solutions of Eq. (40), a convenient way is to impose the following boundary conditions

$$\psi_{\text{even}}(0) = 1, \quad \partial_z \psi_{\text{even}}(0) = 0; \quad (48)$$

$$\psi_{\text{odd}}(0) = 0, \quad \partial_z \psi_{\text{odd}}(0) = 1, \quad (49)$$

where ψ_{even} and ψ_{odd} denote even and odd parity modes of $\psi(z)$, respectively. The integration of the function $|\psi(z)|^2$ can be considered as the probability of finding massive gravitons along the extra dimension. In order to find gravitational resonances, one can define the relative probability [72]:

$$P(m^2) = \frac{\int_{-z_b}^{z_b} |\psi(z)|^2 dz}{\int_{-z_{\max}}^{z_{\max}} |\psi(z)|^2 dz}, \quad (50)$$

where $2z_b$ is the approximate width of the brane and z_{\max} can be taken as $10z_b$. For a given m^2 , using conditions (48) and (49), the even parity mode ψ_{even} and the odd parity mode ψ_{odd} can be solved numerically from the Schrödinger-like equation (40). In this case, the relative probability P corresponding to ψ_{even} or ψ_{odd} can be obtained. As a function of m^2 , the relative probability will have a peak for some value of m^2 . Then we may regard this mode as a gravitational resonance. Actually, we treat it as a resonance only when the corresponding peak has a full width at half maximum Γ , i.e., the width of the half height of the peak value. We can define the lifetime of the gravitational resonance as $\tau = \Gamma^{-1}$.

Next, we will investigate gravitational resonances in three cases. Before that, in order to investigate conveniently we introduce some dimensionless parameters. Using the parameter k , we can define the following dimensionless parameters $\bar{y} = ky$, $\bar{z} = kz$, $\bar{b} = kb$, $\bar{\tau} = k\tau$, $\bar{\Gamma} = \Gamma/k$, $\bar{m} = m/k$, $\bar{W} = W/k^2$, and $\bar{\alpha} = k^2\alpha$. In our system, both parameters \bar{b} and $\bar{\alpha}$ can affect the resonance behavior. The effects of the parameter \bar{b} has been investigated in Refs. [44, 73, 74], so in this paper, we will focus on the effects of the parameter $\bar{\alpha}$, which can measure the deviation from mimetic gravity.

A. Case 1

We begin with the following warp factor

$$a(\bar{y}) = \tanh(\bar{y} + \bar{b}) - \tanh(\bar{y} - \bar{b}). \quad (51)$$

In this case we choose $\bar{b} = 10$ as a specific example to investigate gravitational resonances. So from Eq. (24) we know that $\bar{\alpha}$ has two bounds. Effects of the parameter $\bar{\alpha}$ on the effective potential can be seen from Fig. 9. From

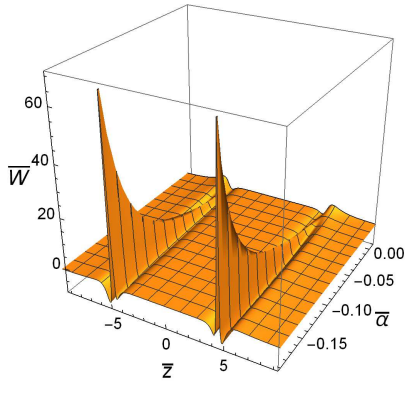


FIG. 9: The effect of the parameter $\bar{\alpha}$ on the effective potential with $\bar{b} = 10$ for case 1.

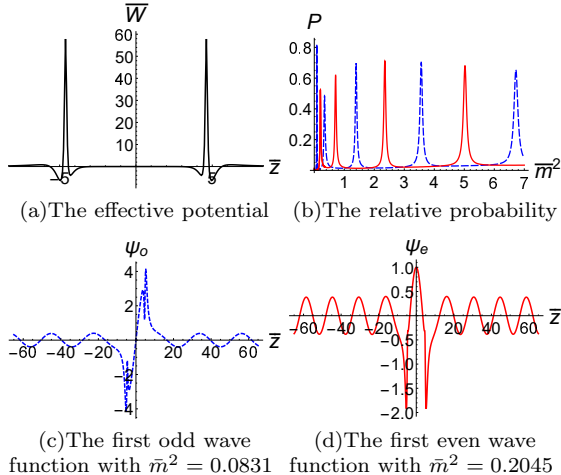


FIG. 10: The effective potential, the relative probability, and the wave functions of the first odd and even resonances with $\bar{b} = 10$ and $\bar{\alpha} = -0.19$ for case 1.

From this figure we can see that, the height of the two big barriers decreases rapidly with $\bar{\alpha}$. When $\bar{\alpha}$ approaches to zero, the barriers will disappear. Besides, the depth of the effective potential will decrease first and then increase with $\bar{\alpha}$.

In this case we set \bar{z}_b in the relative probability (50) as $\bar{z}_b = 6.5$. For $\bar{\alpha} = -0.19, -0.14$, and -0.0012 we can obtain the relative probabilities. Then, the corresponding effective potentials, the relative probabilities, and the wave functions of the first odd and even resonances are shown in Figs. 10, 11, and 12. From Figs. 10(a), 11(a), and 12(a), we can see that, the height of the effective potential barrier decreases with the parameter $\bar{\alpha}$. Besides, from Figs. 10(b) and 11(b) we can see that the peaks values do not decrease with \bar{m}^2 monotonously, which is an unusual phenomenon.

We are also interested in the first gravitational resonance, its lifetime $\bar{\tau}_1$ and the mass square \bar{m}^2 for different values of $\bar{\alpha}$ are shown in Fig. 13. They can be fitted as

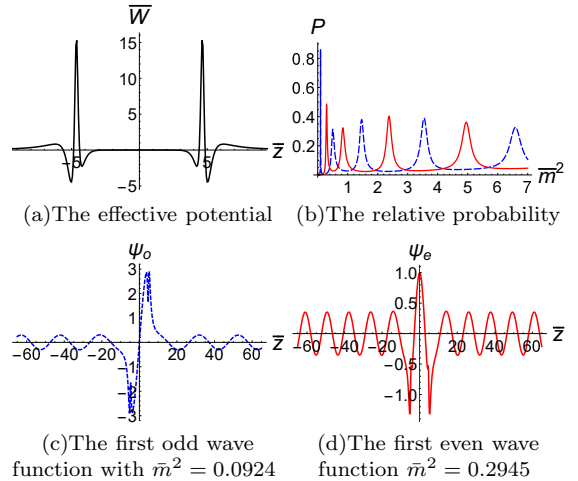


FIG. 11: The effective potential, the relative probability, and the wave functions of the first odd and even resonances with $\bar{b} = 10$ and $\bar{\alpha} = -0.14$ for case 1.

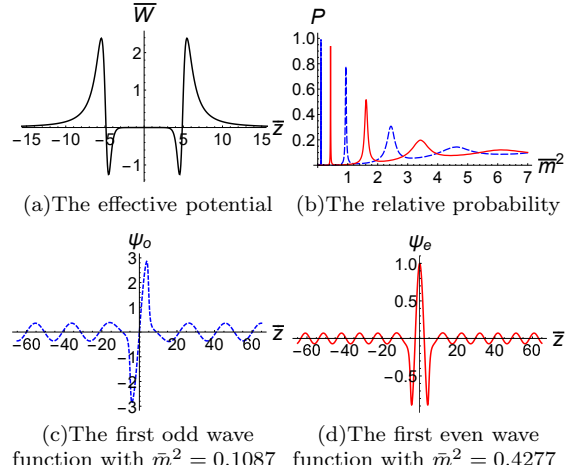


FIG. 12: The effective potential, the relative probability, and the wave functions of the first odd and even resonances with $\bar{b} = 10$ and $\bar{\alpha} = -0.0012$ for case 1.

the following two functions

$$\bar{m}^2 = 0.102\bar{\alpha} + 0.109, \quad (52)$$

$$\bar{\tau}_1 = \frac{1}{0.00335 - 0.447\bar{\alpha}} + 132. \quad (53)$$

From Eq. (52) we can see that the mass square \bar{m}^2 of the first resonance linearly increases with the parameter $\bar{\alpha}$. And from Eq. (53) we can see that the lifetime of the first resonance increases with $\bar{\alpha}$ slowly first and then rapidly when $\bar{\alpha}$ closes to the upper bound.

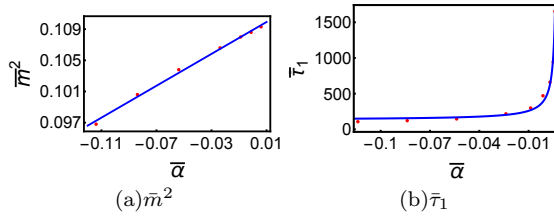


FIG. 13: The effects of the parameter $\bar{\alpha}$ on the mass square \bar{m}^2 and the lifetime $\bar{\tau}$ of the first resonance for case 1. Red dots are numerical results, blue solid lines are fit functions. In the left panel the fit function is $\bar{m}^2 = 0.102\bar{\alpha} + 0.109$, in the right panel the fit function is $\bar{\tau}_1 = \frac{1}{0.00335 - 0.447\bar{\alpha}} + 131.621$.

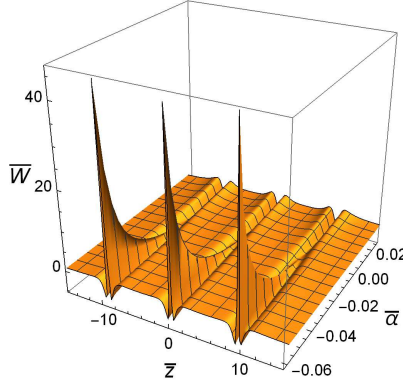


FIG. 14: The effect of the parameter $\bar{\alpha}$ on the effective potential with $\bar{b} = 5$ for case 2.

B. Case 2

In this case, we investigate the brane world with three sub-branes, for which the warp factor is

$$a(\bar{y}) = \operatorname{sech}(\bar{y} - \bar{b}) + \operatorname{sech}(\bar{y}) + \operatorname{sech}(\bar{y} + \bar{b}). \quad (54)$$

Without loss of generality we choose $\bar{b} = 5$ as a specific example, and the corresponding range of $\bar{\alpha}$ is $-0.0642 < \bar{\alpha} < 0.025$. Gravitational resonances also exist in this kind of warp factor, but the situation will be different from case 1. The effective potential for different values of $\bar{\alpha}$ can be seen in Fig. 14. From this figure we can see that there are three sub-wells, and the effect of $\bar{\alpha}$ to the effective potential is similar to that in case 1. We fix $\bar{z}_b = 12$ and set $\bar{\alpha}$ as -0.0581 , -0.0373 , and 0.0161 as examples to study the gravitational resonances.

The shapes of the effective potential, the relative probability and the wave functions of the first odd and even KK resonances are shown in Figs. 15, 16, and 17. We can see that for some values of $\bar{\alpha}$, the relative probabilities of the resonances do not decrease with their masses \bar{m}^2 monotonously, which is similar to case 1. Besides, Figs. 15 and 17 show that the masses of some resonances are very close, which is similar to the result in [31], where the doubly degenerate phenomenon happens. Comparing

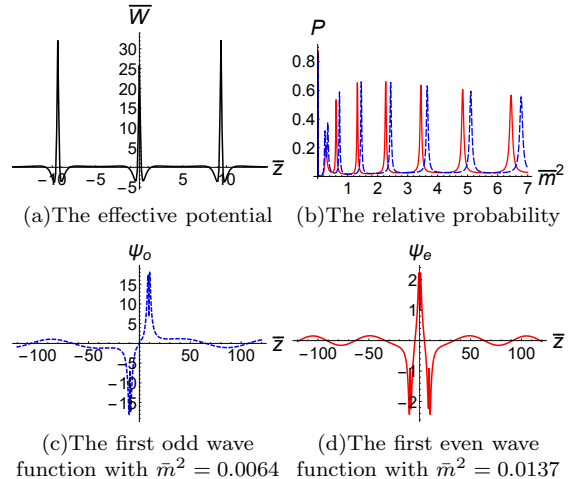


FIG. 15: The effective potential, the relative probability, and wave functions of the first odd and even resonance with $\bar{b} = 5$ and $\bar{\alpha} = -0.0581$ for case 2.

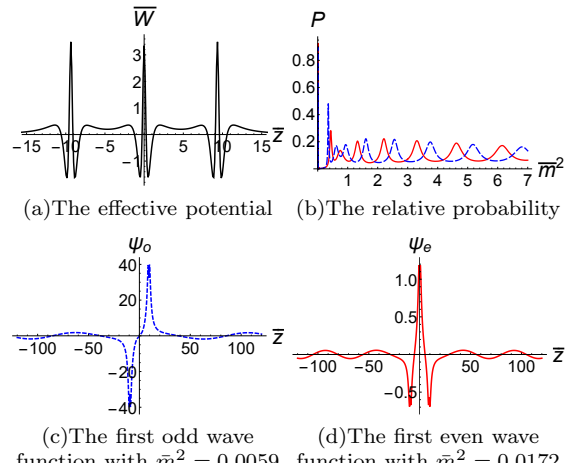


FIG. 16: The effective potential, the relative probability, and wave functions of the first odd and even resonance with $\bar{b} = 5$ and $\bar{\alpha} = -0.0373$ for case 2.

the effective potential with that in Ref. [31], we can see that they both have sub-structure, and this sub-structure is the main reason of this phenomenon.

We also investigate the lifetime $\bar{\tau}_1$ and the mass square \bar{m}^2 of the first resonance for different values of $\bar{\alpha}$. The results are shown in Fig. 18 and we also get the following fit functions

$$\bar{m}^2 = 0.00373 - 0.0557\bar{\alpha}, \quad (55)$$

$$\bar{\tau}_1 = \frac{10000}{14.3 - 540\bar{\alpha}} + 238. \quad (56)$$

From Eq. (55), one can see that the mass square \bar{m}^2 of the first resonance linearly decreases with the parameter $\bar{\alpha}$, which is different from case 1. Equation (56) shows

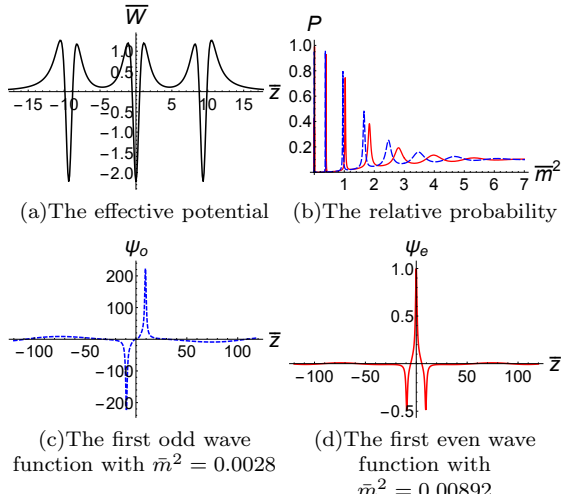


FIG. 17: The effective potential, the relative probability, and wave functions of the first odd and even resonance with $\bar{b} = 5$ and $\bar{\alpha} = 0.016$ for case 2.

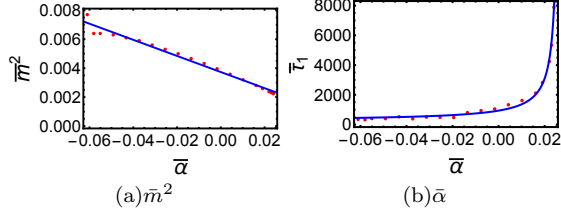


FIG. 18: The effects of $\bar{\alpha}$ to the scaled mass \bar{m}^2 and the scaled lifetime $\bar{\tau}_1$ of the first resonance for case 2. Red dots are numerical results and solid blue lines are fit functions. In the left panel the fit function is $\bar{m}^2 = 0.00373 - 0.0557\bar{\alpha}$, in the right panel the fit function is $\bar{\tau}_1 = \frac{1}{14.3 - 540\bar{\alpha}} + 0.0238$.

that the lifetime increases with $\bar{\alpha}$ slowly first and then rapidly, just like the case 1.

From case 1 and case 2, we find that, when $\bar{\alpha}$ is small, there is an unusual phenomenon, i.e., the peak values of the relative probability of the resonances do not decrease monotonously with \bar{m}^2 . This phenomenon appears when $\bar{\alpha} \lesssim -0.024$ for case 1 and $\bar{\alpha} \lesssim -0.014$ for case 2.

C. Case 3

In this case, we will focus on the gravitational resonances quasi-localized in sub-wells and between sub-wells. The warp factor is

$$a(\bar{y}) = \tanh(\bar{y} - \bar{b} - \bar{d}) - \tanh(\bar{y} + \bar{b} + \bar{d}) - \tanh(\bar{y} + \bar{d}) + \tanh(\bar{y} - \bar{d}). \quad (57)$$

Compared with case 1, this warp factor has two platforms and the effective potential has more abundant sub-structure, which can be seen in Fig. 19.

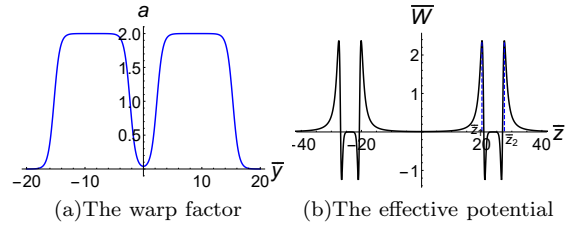


FIG. 19: The warp factor and the effective potential $W(\bar{z})$ for case 3. The parameters are set as $\bar{b} = 13$, $\bar{d} = 2.3$, and $\bar{\alpha} = -0.00126$.

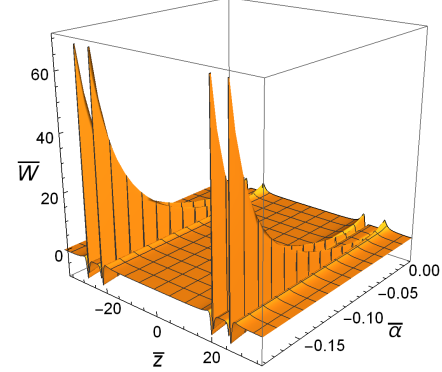


FIG. 20: The effect of the parameter $\bar{\alpha}$ on the effective potential with $\bar{b} = 13$ and $\bar{d} = 2.3$ for case 3.

From case 1 we have found that for large \bar{b} the range of $\bar{\alpha}$ is $-0.219 < \bar{\alpha} < 0.00625$. In the current case we set $\bar{b} = 13$ and $\bar{d} = 2.3$, for which the range of $\bar{\alpha}$ is still $-0.219 < \bar{\alpha} < 0.00625$.

The effective potential for different values of $\bar{\alpha}$ is shown in Fig. 20. In order to investigate the resonances only quasi-localized in sub-wells, we need to redefine the corresponding relative probability P_s [44]:

$$P_s = \begin{cases} \frac{\int_{\bar{z}_1}^{\bar{z}_2} |\psi(\bar{z})|^2 d\bar{z}}{\int_{\bar{z}_m+5(\bar{z}_2-\bar{z}_1)}^{\bar{z}_m+5(\bar{z}_2-\bar{z}_1)} |\psi(\bar{z})|^2 d\bar{z}}, & \bar{z}_m \geq 5(\bar{z}_2 - \bar{z}_1) \\ \frac{\int_{\bar{z}_1}^{\bar{z}_2} |\psi(\bar{z})|^2 d\bar{z}}{\int_0^{10(\bar{z}_2-\bar{z}_1)} |\psi(\bar{z})|^2 d\bar{z}}, & \bar{z}_m < 5(\bar{z}_2 - \bar{z}_1) \end{cases} \quad (58)$$

where \bar{z}_1 and \bar{z}_2 are the left and right edges of the right sub-well respectively (as Fig. 19(b) shows), and $\bar{z}_m = \frac{\bar{z}_1 + \bar{z}_2}{2}$. Besides, between two sub-wells there is also a potential well, and resonances can also be quasi-localized in it. We also need to redefine the relative probability in this region [44]:

$$P_m = \frac{\int_{-\bar{z}_1}^{\bar{z}_1} |\psi(\bar{z})|^2 d\bar{z}}{\int_{-10\bar{z}_1}^{10\bar{z}_1} |\psi(\bar{z})|^2 d\bar{z}}. \quad (59)$$

We solve the Shrödinger-like equation (40) numerically with the boundary conditions (48) and (49). Using the

redefined relative probabilities (58) and (59), one can get the gravitational resonances. Figures 21, 23, and 25 show the effective potential and the corresponding relative probability for $\bar{\alpha} = -0.189$, $\bar{\alpha} = -0.0838$, and $\bar{\alpha} = -0.00126$, respectively. Through these figures we can see that the effects of $\bar{\alpha}$ on the effective potentials and relative probability are very considerable. Compared with the results of mimetic gravity brane world (see Fig. 11(c) in Ref. [44]), we find that relative probabilities of resonances in sub-wells for small $\bar{\alpha}$ are much larger, which can be seen in Fig. 21(c). As $\bar{\alpha}$ approaches to zero, mimetic $f(R)$ gravity will go back to mimetic gravity and the results of gravitational resonances will also recover to that of in mimetic gravity [44].

From Figs. 21(c), 23(c), and 25(c) we can see that the peaks of relative probabilities of gravitational resonances in the sub-wells appear in clusters. And the main peak value of each cluster does not monotonically decrease with \bar{m}^2 when $\bar{\alpha}$ is small, this is because the sub-wells also have their sub-structure changing with $\bar{\alpha}$. From Figs. 21(b), 23(b), and 25(b) we can also see that the peak values of relative probabilities of gravitational resonances quasi-localized between sub-wells will not monotonically decrease with \bar{m}^2 . Besides, comparing the above two cases, we see that there are no corresponding resonances with large relative probabilities P_m at the locations of the main peaks of clusters in P_s . This is caused by the existence of sub-structure of the effective potential. The wave functions of resonances quasi-localized both between sub-wells and in sub-wells are shown in Figs. 22, 24, and 26 for corresponding $\bar{\alpha}$.

On the other hand, from Figs. 21(c), 23(c), and 25(c) we find that the mass square \bar{m}^2 of the first odd parity resonance and the first even parity resonance are very close. One could also regard this as doubly degenerate [31].

V. CONCLUSIONS AND DISCUSSION

In this work, we studied the brane world system in mimetic $f(R)$ gravity. Due to the existence of the mimetic scalar field, we can get thick branes with abundant inner structure. We gave three kinds of solutions of the thick brane model for $f(R) = R + \alpha R^2$.

Then we investigated the stability of mimetic $f(R)$ brane world, and found that the system is stable under the tenser perturbation. The existence of the normalized graviton zero mode indicates that four-dimensional gravity can be restored. Besides, the result is same as the tensor perturbation of $f(R)$ -branes in Ref. [71], this is because that the tenser perturbation is independent of the mimetic scalar field.

After that, we studied the gravitational resonances, which are quasi-localized on the brane. We only studied the effects of the parameter α on the behavior of the resonances. We found that for a small α , the effective potential has a sub-structure which leads to an unusual

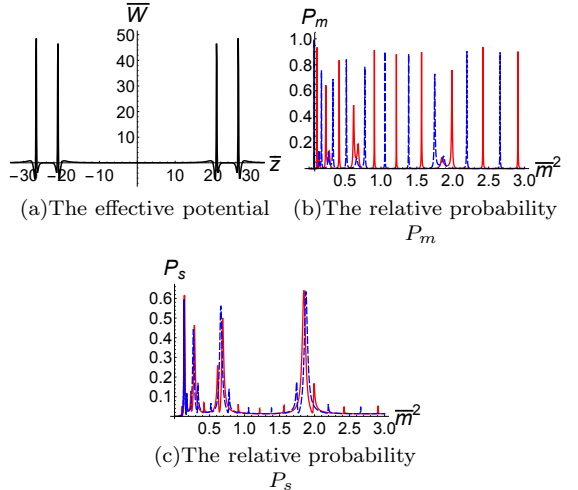


FIG. 21: The effective potential, the relative probabilities of the even parity mode ψ_e (dashed blue lines) and the odd parity mode ψ_o (solid red lines) quasi-localized between the sub-wells P_m and in the sub-wells P_s with $\bar{b} = 13$, $\bar{d} = 2.3$, and $\bar{\alpha} = -0.189$ for case 3.

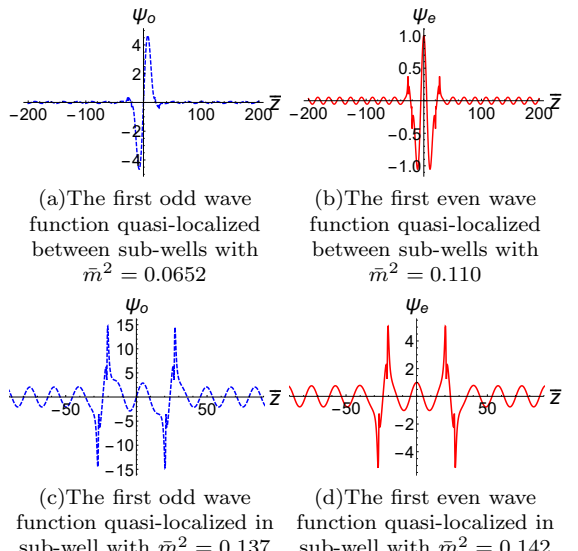


FIG. 22: Resonances quasi-localized between sub-wells and in sub-wells with $\bar{b} = 13$, $\bar{d} = 2.3$, and $\bar{\alpha} = -0.189$ for case 3.

phenomenon in the resonance spectrum. The lifetime of the first resonance increases rapidly while α close to its upper bound. In case 3 we focused on gravitational resonances quasi-localized in sub-wells and between sub-wells, and found that resonances can be quasi-localized both in sub-wells and between sub-wells. If α tends to zero the result would tend to mimetic gravity brane world in Ref. [44]. Compared with Ref. [44], the relative probabilities of resonances in the sub-wells are more obvious and the main peak values of the clusters do not monotonically decrease with \bar{m}^2 for a small α . Besides, the phe-

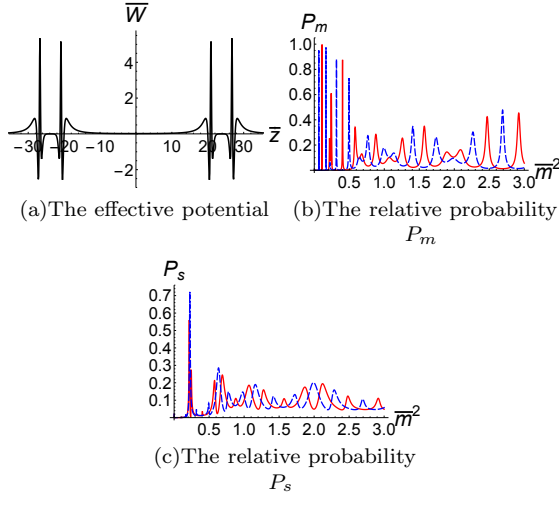


FIG. 23: The effective potential, the relative probabilities of the even parity mode ψ_e (dashed blue lines) and the odd parity mode ψ_o (solid red lines) quasi-localized between the sub-wells P_m and in the sub-wells P_s with $\bar{b} = 13$, $\bar{d} = 2.3$, and $\bar{\alpha} = -0.0838$ for case 3.

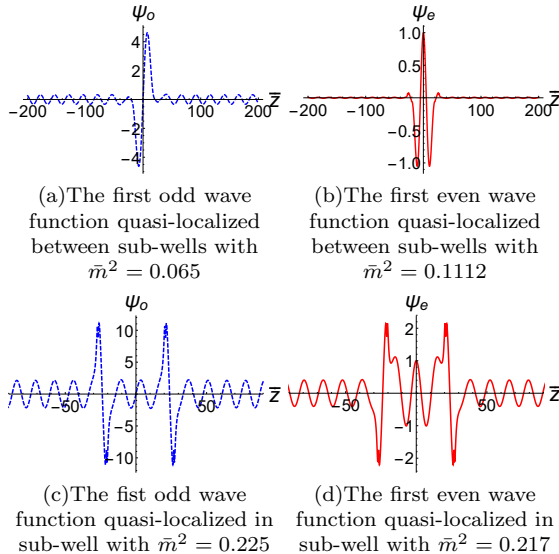


FIG. 24: Resonances between sub-wells and in a sub-well with $\bar{b} = 13$, $\bar{d} = 2.3$, and $\bar{\alpha} = -0.0838$ for case 3.

nomenon of gravitational resonance doubly degenerate also appears when we studied resonances quasi-localized in a sub-well.

In the model of mimetic brane world with abundant inner structure, it is also interesting to investigate localization of various kinds of matter fields and the corresponding resonance structures, which will be studied in our future work.

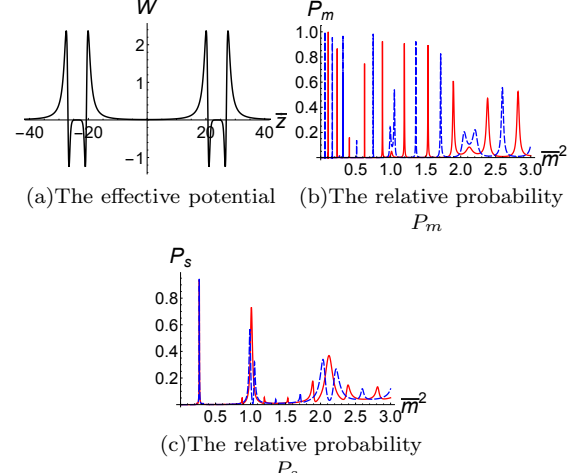


FIG. 25: The effective potential, the relative probabilities of the even parity mode ψ_e (dashed blue lines) and the odd parity mode ψ_o (solid red lines) quasi-localized between the sub-wells P_m and in the sub-wells P_s with $\bar{b} = 13$, $\bar{d} = 2.3$, and $\bar{\alpha} = -0.00126$ for case 3.

VI. ACKNOWLEDGENTS

We would like thank Yi Zhong for useful discussions. This work was supported in part by the National Natural Science Foundation of China (Grants No. 11875151 and No. 11522541) and the Fundamental Research Funds for the Central Universities (Grants No. lzujbky-2019-ct06). W. D. Guo was supported by the scholarship granted by the Chinese Scholarship Council (CSC).

[1] N. Arkani-Hamed, S. Dimopoulos, and G. Dvali, *The hierarchy problem and new dimensions at a millimeter*, *Phys. Lett. Sect. B Nucl. Elem. Part. High-Energy Phys.* **429** (1998), no. 3-4 263–272, [[arXiv:hep-ph/9803315](https://arxiv.org/abs/hep-ph/9803315)].

[2] L. Randall and R. Sundrum, *A Large Mass Hierarchy from a Small Extra Dimension*, *Phys. Rev. Lett.* **83** (1999), no. 17 1–4.

[3] L. Randall and R. Sundrum, *An alternative to compactification*, *Phys. Rev. Lett.* **83** (1999), no. 23 4690–4693.

[4] V. A. Rubakov and M. E. Shaposhnikov, *Do we live inside a domain wall?*, *Phys. Lett. B* **125** (1983), no. 2 136–138.

[5] O. DeWolfe, D. Z. Freedman, S. S. Gubser, and A. Karch, *Modeling the fifth dimension with scalars and gravity*, *Phys. Rev. D - Part. Fields, Gravit. Cosmol.* **62** (2000), no. 4 16, [[arXiv:hep-th/9909134](https://arxiv.org/abs/hep-th/9909134)].

[6] C. Csaki, J. Erlich, T. J. Hollowood, and Y. Shirman, *Universal aspects of gravity localized on thick*

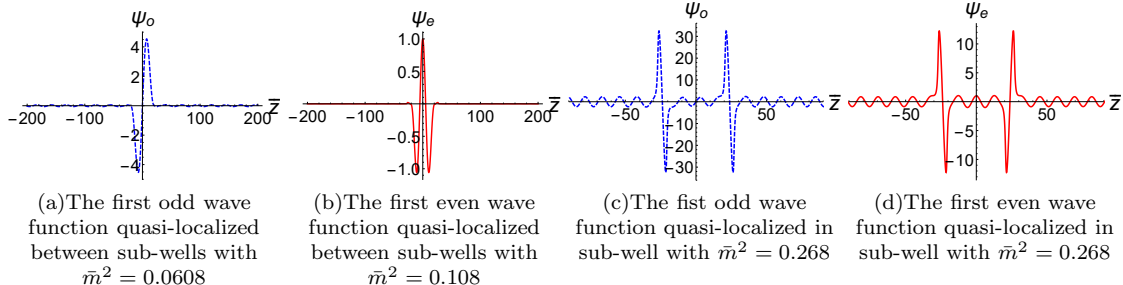


FIG. 26: Resonances between sub-wells and in a sub-well with $\bar{b} = 13$, $\bar{d} = 2.3$, and $\bar{\alpha} = -0.00126$ for case 3.

branes, *Nucl. Phys. B* **581** (2000), no. 1-2 309–338, [[arXiv:hep-th/0001033](#)].

[7] M. Gremm, *Four-dimensional gravity on a thick domain wall*, *Phys. Lett. Sect. B Nucl. Elem. Part. High-Energy Phys.* **478** (2000), no. 4 434–438, [[arXiv:hep-th/9912060](#)].

[8] A. Kehagias and K. Tamvakis, *Localized gravitons, gauge bosons and chiral fermions in smooth spaces generated by a bounce*, *Phys. Lett. Sect. B Nucl. Elem. Part. High-Energy Phys.* **504** (2001), no. 1-2 38–46, [[arXiv:hep-th/0010112](#)].

[9] A. Melfo, N. Pantoja, and J. D. Tempo, *Fermion localization on thick branes*, *Phys. Rev. D - Part. Fields, Gravit. Cosmol.* **73** (2006), no. 4 [[arXiv:hep-th/0601161](#)].

[10] Q.-Y. Xie, H. Guo, Z.-H. Zhao, Y.-Z. Du, and Y.-P. Zhang, *Spectrum structure of a fermion on Bloch branes with two scalar-fermion couplings*, *Class. Quantum Gravity* **34** (2017), no. 5 [[arXiv:1510.03345](#)].

[11] A. E. R. Chumbes, A. E. O. Vasquez, and M. B. Hott, *Fermion localization on a split brane*, *Phys. Rev. D - Part. Fields, Gravit. Cosmol.* **83** (2011), no. 10 1–17, [[arXiv:1012.1480](#)].

[12] Z.-H. Zhao, Y.-X. Liu, and H.-T. Li, *Fermion localization on asymmetric two-field thick branes*, *Class. Quantum Gravity* **27** (2010), no. 18 [[arXiv:0911.2572](#)].

[13] C. A. Almeida, R. Casana, M. M. Ferreira, and A. R. Gomes, *Fermion localization and resonances on two-field thick branes*, *Phys. Rev. D - Part. Fields, Gravit. Cosmol.* **79** (2009), no. 12 1–24, [[arXiv:0901.3543](#)].

[14] X.-N. Zhou, Y.-Z. Du, H. Yu, and Y.-X. Liu, *Localization of gravitino field on $f(R)$ -thick branes*, *Sci. China Physics, Mech. Astron.* **61** (2018), no. 11 [[arXiv:1703.10805](#)].

[15] Y.-X. Liu, Y. Zhong, Z.-H. Zhao, and H.-T. Li, *Domain wall brane in squared curvature gravity*, *J. High Energy Phys.* **2011** (2011), no. 6 [[arXiv:1104.3188v2](#)].

[16] P. Binétruy, C. Deffayet, and D. Langlois, *Non-conventional cosmology from a brane universe*, *Nucl. Phys. B* **565** (2000), no. 1-2 269–287.

[17] P. Binétruy, C. Deffayet, U. Ellwanger, and D. Langlois, *Brane cosmological evolution in a bulk with cosmological constant*, *Phys. Lett. Sect. B Nucl. Elem. Part. High-Energy Phys.* **477** (2000), no. 1-3 285–291, [[arXiv:hep-th/9910219](#)].

[18] A. Kamenshchik, U. Moschella, and V. Pasquier, *An alternative to quintessence*, *Phys. Lett. Sect. B Nucl. Elem. Part. High-Energy Phys.* **511** (2001), no. 2-4 265–268, [[arXiv:gr-qc/0103004](#)].

[19] Y. Zhong, C.-E. Fu, and Y.-X. Liu, *Cosmological twinlike models with multi scalar fields*, *Sci. China Physics, Mech. Astron.* **61** (2018), no. 9 1–6, [[arXiv:1604.06857](#)].

[20] C. Csáki, M. Graesser, L. Randall, and J. Terning, *Cosmology of brane models with radion stabilization*, *Phys. Rev. D - Part. Fields, Gravit. Cosmol.* **62** (2000), no. 4 19, [[arXiv:hep-ph/9911406](#)].

[21] P. Brax and G. Van de Bruck, *Cosmology and brane worlds: A review*, *Class. Quantum Gravity* **20** (2003), no. 9 [[arXiv:hep-th/0303095](#)].

[22] Y.-X. Liu, *Introduction to extra dimensions and thick braneworlds*, in *Meml. Vol. Yi-shi Duan*, pp. 211–275. 2018. [arXiv:1707.08541](#).

[23] Y.-X. Liu, K. Yang, H. Guo, and Y. Zhong, *Domain wall brane in Eddington-inspired Born-Infeld gravity*, *Phys. Rev. D - Part. Fields, Gravit. Cosmol.* **85** (2012), no. 12 1–16, [[arXiv:1203.2349](#)].

[24] Z.-G. Xu, Y. Zhong, H. Yu, and Y.-X. Liu, *The structure of $f(R)$ -brane model*, *Eur. Phys. J. C* **75** (2015), no. 8 368, [[arXiv:1405.6277](#)].

[25] H. Yu, Y. Zhong, B.-M. Gu, and Y.-X. Liu, *Gravitational resonances on $f(R)$ -brane*, *Eur. Phys. J. C* **76** (2016), no. 4.

[26] W. T. da Cruz, D. M. Dantas, R. V. Maluf, and C. A. S. Almeida, *Configurational Entropy and Newton’s Law in Double Sine-Gordon Braneworlds*, *Ann. Phys.* **531** (2019), no. 10 1–17, [[arXiv:1810.03991](#)].

[27] J.-J. Wan, Z.-Q. Cui, W.-B. Feng, and Y.-X. Liu, *Smooth Braneworld in 6-Dimensional Asymptotically AdS Spacetime*. [arXiv:2010.05016](#).

[28] D. Bazeia and A. R. Gomes, *Bloch brane*, *J. High Energy Phys.* **8** (2004), no. 5 233–245, [[arXiv:hep-th/0403141](#)].

[29] A. De Souza Dutra, A. C. Amaro De Faria, and M. Hott, *Degenerate and critical Bloch branes*, *Phys. Rev. D - Part. Fields, Gravit. Cosmol.* **78** (2008), no. 4 1–18, [[arXiv:0807.0586](#)].

[30] A. D. S. Dutra, G. P. De Brito, and J. M. Da Silva, *Method for obtaining thick brane models*, *Phys. Rev. D - Part. Fields, Gravit. Cosmol.* **91** (2015), no. 8 [[arXiv:1412.5543](#)].

[31] Q.-Y. Xie, Z.-H. Zhao, J. Yang, and K. Yang, *Fermion localization and degenerate resonances on brane array*, *Class. Quantum Gravity* **37** (2020), no. 2 1–21, [[arXiv:1901.11253](#)].

[32] Planck Collaboration XVI, *Planck 2013 results. XVI. Cosmological parameters*, *Astron. Astrophys.* **571** (2014) 1–69, [[arXiv:1303.5076](#)].

[33] Supernova Search Team, *Observational Evidence from*

Supernovae for an Accelerating Universe and a Cosmological Constant, *Astron. J.* **116** (1998), no. 3 1009–1038, [[arXiv:astro-ph/9805201](https://arxiv.org/abs/astro-ph/9805201)].

[34] E. Corbelli and P. Salucci, *The extended rotation curve and the dark matter halo of M33*, *Mon. Not. R. Astron. Soc.* **311** (2000), no. 2 441–447, [[arXiv:astro-ph/9909252v1](https://arxiv.org/abs/astro-ph/9909252v1)].

[35] A. H. Chamseddine and V. Mukhanov, *Mimetic dark matter*, *J. High Energy Phys.* **2013** (2013), no. 11 1–4, [[arXiv:1308.5410](https://arxiv.org/abs/1308.5410)].

[36] A. H. Chamseddine, V. Mukhanov, and A. Vikman, *Cosmology with mimetic matter*, *J. Cosmol. Astropart. Phys.* **2014** (2014), no. 6 [[arXiv:1403.3961](https://arxiv.org/abs/1403.3961)].

[37] F. Capela and S. Ramazanov, *Modified dust and the small scale crisis in CDM*, *J. Cosmol. Astropart. Phys.* **2015** (2015), no. 4 [[arXiv:1412.2051](https://arxiv.org/abs/1412.2051)].

[38] L. Mirzagholi and A. Vikman, *Imperfect Dark Matter*, *J. Cosmol. Astropart. Phys.* **2015** (2015), no. 6 [[arXiv:1412.7136](https://arxiv.org/abs/1412.7136)].

[39] E. Babichev and S. Ramazanov, *Gravitational focusing of imperfect dark matter*, *Phys. Rev. D* **95** (2017), no. 2 1–18, [[arXiv:1609.08580](https://arxiv.org/abs/1609.08580)].

[40] A. Golovnev, *On the recently proposed mimetic Dark Matter*, *Phys. Lett. Sect. B Nucl. Elem. Part. High-Energy Phys.* **728** (2014), no. 5 39–40, [[arXiv:1310.2790](https://arxiv.org/abs/1310.2790)].

[41] A. O. Barvinsky, *Dark matter as a ghost free conformal extension of Einstein theory*, *J. Cosmol. Astropart. Phys.* **2014** (2014), no. 1 1–8, [[arXiv:1311.3111](https://arxiv.org/abs/1311.3111)].

[42] N. Deruelle and J. Rua, *Disformal transformations, veiled general relativity and mimetic gravity*, *J. Cosmol. Astropart. Phys.* **2014** (2014), no. 9 1–5, [[arXiv:1407.0825](https://arxiv.org/abs/1407.0825)].

[43] Y. Zhong, Y. Zhong, Y.-P. Zhang, and Y.-X. Liu, *Thick branes with inner structure in mimetic gravity*, *Eur. Phys. J. C* **78** (2018), no. 1 1–8, [[arXiv:1711.09413](https://arxiv.org/abs/1711.09413)].

[44] Y. Zhong, Y.-P. Zhang, W.-D. Guo, and Y.-X. Liu, *Gravitational resonances in mimetic thick branes*, *J. High Energy Phys.* **2019** (2019), no. 4 [[arXiv:1812.06453v1](https://arxiv.org/abs/1812.06453v1)].

[45] K. S. Stelle, *Renormalization of higher-derivative quantum gravity*, *Phys. Rev. D* **16** (1977), no. 4 953–969.

[46] T. P. Sotiriou and V. Faraoni, *$F(R)$ theories of gravity*, *Rev. Mod. Phys.* **82** (mar, 2010) 451–497, [[arXiv:0805.1726](https://arxiv.org/abs/0805.1726)].

[47] S. Nojiri and S. D. Odintsov, *Unifying inflation with Λ CDM epoch in modified $f(R)$ gravity consistent with Solar System tests*, *Phys. Lett. Sect. B Nucl. Elem. Part. High-Energy Phys.* **657** (2007), no. 4–5 238–245, [[arXiv:0707.1941](https://arxiv.org/abs/0707.1941)].

[48] G. Cognola, E. Elizalde, S. Nojiri, S. D. Odintsov, L. Sebastiani, and S. Zerbini, *Class of viable modified $f(R)$ gravities describing inflation and the onset of accelerated expansion*, *Phys. Rev. D - Part. Fields, Gravit. Cosmol.* **77** (2008), no. 4 1–15, [[arXiv:0712.4017](https://arxiv.org/abs/0712.4017)].

[49] S. Nojiri and S. D. Odintsov, *Modified $f(R)$ gravity unifying Rm inflation with the Λ CDM epoch*, *Phys. Rev. D - Part. Fields, Gravit. Cosmol.* **77** (2008), no. 2 [[arXiv:0710.1738](https://arxiv.org/abs/0710.1738)].

[50] Q.-G. Huang, *A polynomial $f(R)$ inflation model*, *J. Cosmol. Astropart. Phys.* **2014** (2014), no. 2 1–5, [[arXiv:1309.3514](https://arxiv.org/abs/1309.3514)].

[51] D. J. Brooker, S. D. Odintsov, and R. P. Woodard, *Precision predictions for the primordial power spectra from $f(R)$ models of inflation*, *Nucl. Phys. B* **911** (2016) 318–337, [[arXiv:1606.05879](https://arxiv.org/abs/1606.05879)].

[52] L. Sebastiani and R. Myrzakulov, *$F(R)$ -gravity and inflation*, 2015.

[53] S. Capozziello, V. F. Cardone, and A. Troisi, *Reconciling dark energy models with $f(R)$ theories*, *Phys. Rev. D - Part. Fields, Gravit. Cosmol.* **71** (2005), no. 4 1–15, [[arXiv:astro-ph/0501426](https://arxiv.org/abs/astro-ph/0501426)].

[54] M. Amarzguioui, Elgarøy, D. F. Mota, and T. Multamäki, *Cosmological constraints on $f(R)$ gravity theories within the Palatini approach*, *Astron. Astrophys.* **454** (2006), no. 3 707–714.

[55] T. Faulkner, M. Tegmark, E. F. Bunn, and Y. Mao, *Constraining $f(R)$ gravity as a scalar-tensor theory*, *Phys. Rev. D - Part. Fields, Gravit. Cosmol.* **76** (2007), no. 6 1–15, [[arXiv:astro-ph/0612569](https://arxiv.org/abs/astro-ph/0612569)].

[56] Y.-S. Song, W. Hu, and I. Sawicki, *Large scale structure of $f(R)$ gravity*, *Phys. Rev. D - Part. Fields, Gravit. Cosmol.* **75** (2007), no. 4 1–10, [[arXiv:astro-ph/0610532](https://arxiv.org/abs/astro-ph/0610532)].

[57] A. A. Starobinsky, *Disappearing cosmological constant in $f(R)$ gravity*, *JETP Lett.* **86** (2007), no. 3 157–163, [[arXiv:0706.2041](https://arxiv.org/abs/0706.2041)].

[58] W. Hu and I. Sawicki, *Models of $f(R)$ cosmic acceleration that evade solar system tests*, *Phys. Rev. D - Part. Fields, Gravit. Cosmol.* **76** (2007), no. 6 1–13, [[arXiv:0705.1158](https://arxiv.org/abs/0705.1158)].

[59] O. Bertolami, C. G. Böhmer, T. Harko, and F. S. Lobo, *Extra force in $f(R)$ modified theories of gravity*, *Phys. Rev. D - Part. Fields, Gravit. Cosmol.* **75** (2007), no. 10 [[arXiv:0704.1733](https://arxiv.org/abs/0704.1733)].

[60] L. Amendola, R. Gannouji, D. Polarski, and S. Tsujikawa, *Conditions for the cosmological viability of $f(R)$ dark energy models*, *Phys. Rev. D - Part. Fields, Gravit. Cosmol.* **75** (2007), no. 8 [[arXiv:gr-qc/0612180](https://arxiv.org/abs/gr-qc/0612180)].

[61] R. Bean, D. Bernat, L. Pogosian, A. Silvestri, and M. Trodden, *Dynamics of linear perturbations in $f(R)$ gravity*, *Phys. Rev. D - Part. Fields, Gravit. Cosmol.* **75** (2007), no. 6 1–15, [[arXiv:astro-ph/0611321](https://arxiv.org/abs/astro-ph/0611321)].

[62] S. D. Odintsov, *Mimetic $F(R)$ gravity: Inflation, dark energy and bounce*, *Mod. Phys. Lett. A* **29** (2014), no. 40 1–13.

[63] G. Leon and E. N. Saridakis, *Dynamical behavior in mimetic $F(R)$ gravity*, *J. Cosmol. Astropart. Phys.* **2015** (2015), no. 4 [[arXiv:1501.00488](https://arxiv.org/abs/1501.00488)].

[64] S. D. Odintsov and V. K. Oikonomou, *Dark energy oscillations in mimetic $F(R)$ gravity*, *Phys. Rev. D* **94** (2016), no. 4 1–14, [[arXiv:1608.00165v1](https://arxiv.org/abs/1608.00165v1)].

[65] N. Myrzakulov, *Stability of de Sitter solution in mimetic $f(R)$ gravity*, *J. Phys. Conf. Ser.* **633** (2015), no. 1.

[66] K. Nozari and N. Sadeghnezhad, *Braneworld mimetic $f(R)$ gravity*, *Int. J. Geom. Methods Mod. Phys.* (2019) 1950042.

[67] W.-D. Guo, Y. Zhong, K. Yang, T.-T. Sui, and Y.-X. Liu, *Thick brane in mimetic $f(T)$ gravity*, *Phys. Lett. Sect. B Nucl. Elem. Part. High-Energy Phys.* **800** (2020) [[arXiv:1805.05650](https://arxiv.org/abs/1805.05650)].

[68] J. L. Rosa, D. A. Ferreira, D. Bazeia, and F. S. N. Lobo, *Thick brane structures in generalized hybrid metric-Palatini gravity*, [[arXiv:2010.10074](https://arxiv.org/abs/2010.10074)].

[69] A. V. Astashenok, S. D. Odintsov, and V. K. Oikonomou, *Modified Gauss-Bonnet gravity with the Lagrange multiplier constraint as mimetic theory*, *Class. Quantum Gravity* **32** (2015), no. 18 0–24, [[arXiv:1504.04861](https://arxiv.org/abs/1504.04861)].

[70] J. Soda and K. Koyama, *Thick brane worlds and their stability*, *Phys. Rev. D - Part. Fields, Gravit. Cosmol.*

65 (2002), no. 6 9, [[arXiv:arXiv:hep-th/0107025v4](https://arxiv.org/abs/hep-th/0107025v4)].

[71] Y. Zhong, Y.-X. Liu, and K. Yang, *Tensor perturbations of $f(R)$ -branes*, *Phys. Lett. Sect. B Nucl. Elem. Part. High-Energy Phys.* **699** (2011), no. 5 398–402, [[arXiv:hep-th/1010.3478](https://arxiv.org/abs/hep-th/1010.3478)].

[72] Y.-X. Liu, J. Yang, Z.-H. Zhao, C.-E. Fu, and Y.-S. Duan, *Fermion localization and resonances on a de Sitter thick brane*, *Phys. Rev. D - Part. Fields, Gravit. Cosmol.* **80** (2009), no. 6 1–13.

[73] Q.-M. Fu, L. Zhao, K. Yang, B.-M. Gu, and Y.-X. Liu, *Stability and (quasi)localization of gravitational fluctuations in an Eddington-inspired Born-Infeld brane system*, *Phys. Rev. D - Part. Fields, Gravit. Cosmol.* **90** (2014), no. 10 12–14, [[arXiv:1407.6107](https://arxiv.org/abs/1407.6107)].

[74] Q. Tan, W.-D. Guo, Y.-P. Zhang, and Y.-X. Liu, *Gravitational resonances on $f(T)$ -branes*, [[arXiv:2008.08440](https://arxiv.org/abs/2008.08440)].